

Review

# The Kuroshio Extension System: Its Large-Scale Variability and Role in the Midlatitude Ocean-Atmosphere Interaction

Bo QIU\*

Department of Oceanography, University of Hawaii at Manoa, Honolulu, HI 96822, U.S.A.

(Received 8 April 2001; in revised form 30 July 2001; accepted 30 July 2001)

**The Kuroshio Extension and its recirculation gyre form an interconnected dynamic system. The system is located at a crossroads where the meso-scale and large-scale oceanic variability are highest, and where the ocean-atmosphere interaction is most active in the Pacific Ocean outside of the tropics. Following a brief review of the mean flow and meso-scale eddy variability, this study describes in detail the large-scale structural change (an oscillation between an elongated and a contracted state) observed in the Kuroshio Extension system. Causes for this structural change are explored next, and it is argued that the basin-wide external wind forcing and the nonlinear dynamics associated with the inertial recirculation gyre are both important factors. Data analysis results are reviewed and presented, emphasizing that the surface Kuroshio Extension is *not* simply a well-mixed layer passively responding to heat flux anomalies imposed by the atmosphere. It is argued that large-scale changes in the Kuroshio Extension system influence the surface ocean heat balance and generate wintertime sea surface temperature (SST) anomalies through both horizontal geostrophic heat advection *and* re-emergence to the surface mixed layer of sequestered mode water temperature anomalies.**

Keywords:

- Kuroshio Extension,
- recirculation gyre,
- mixed layer heat balance,
- obduction,
- midlatitude ocean-atmosphere coupling.

## 1. Introduction

The Kuroshio Extension is the region of the North Pacific Ocean occupied by the Kuroshio after it separates from the coast of Japan near 140°E and 35°N (Kawai, 1972). Figure 1, from Mizuno and White (1983), shows the mean temperature map at 300 m depth, in which the axis of the Kuroshio Extension is well represented by the 12°C isotherm. An interesting feature in the upstream Kuroshio Extension east of Japan is the presence of two quasi-stationary meanders with their ridges located at 144°E and 150°E, respectively. The existence of the quasi-stationary meanders as a *mean* circulation feature of the Kuroshio Extension can also be seen in the sea surface dynamic height maps constructed from historical hydrographic data (e.g., Wyrski, 1975; Teague *et al.*, 1990; Qu *et al.*, 2001) and from satellite altimeter data (Fig. 2). In their 1983 study, Mizuno and White interpreted the two quasi-stationary meanders as standing Rossby lee

waves induced by the presence of the Izu Ridge (see Fig. 2 for the major bottom topography in the region). In contrast, a recent modeling study by Hurlburt *et al.* (1996) argued that the quasi-stationary meanders are steered by the eddy-driven abyssal mean flows resulting from instability of the Kuroshio Extension jet.

Near 159°E, the Kuroshio Extension encounters the Shatsky Rise where the eastward flow often bifurcates: the main body of the Kuroshio Extension continues eastward, and a secondary branch tends to extend northeastward to 40°N, where it joins the eastward flowing Subarctic Current (Fig. 1). After overriding the Emperor Seamounts along 171°E, the mean path of the Kuroshio Extension becomes broadened and instantaneous flow patterns often show a multiple-jet structure associated with the eastward flowing Kuroshio Extension (e.g., Joyce, 1987; Joyce and Schmitz, 1988; Roden, 1998). East of the dateline, the distinction between the Kuroshio Extension and the Subarctic Current is no longer clear, and together they form the broad, eastward-moving North Pacific Current.

\* E-mail address: bo@soest.hawaii.edu

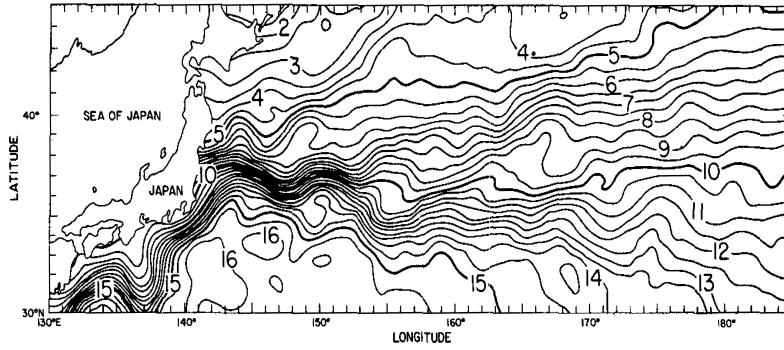


Fig. 1. Mean temperature map ( $^{\circ}\text{C}$ ) at the 300 m depth from 1976 to 1980. Adapted from Mizuno and White (1983).

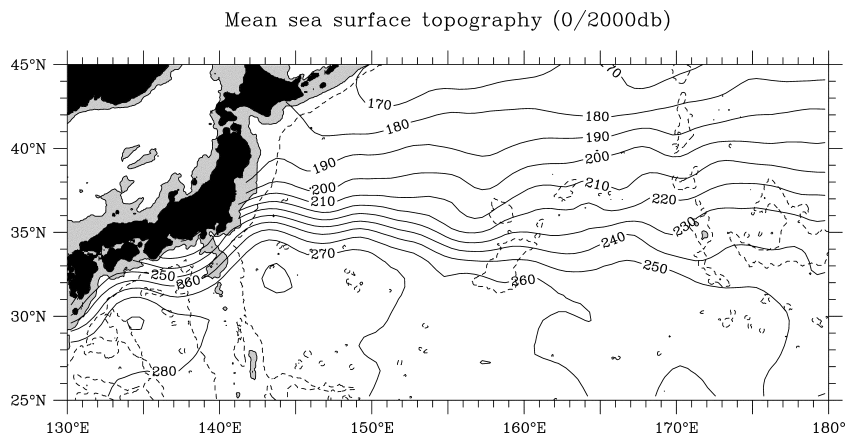


Fig. 2. Sea surface topography (in meters) relative to 2000 dbar by merging the T/P reconstructed mean SSH field and the Levitus (1982) climatology. Adapted from Qiu (2000). Dashed lines denote the 4000-m isobaths, and areas shallower than 1000 m are shaded. Major bathymetric features in the region include the Izu-Ogasawara Ridge along  $141^{\circ}\text{E}$ , the Shatsky Rise near  $159^{\circ}\text{E}$ , and the Emperor Seamounts along  $172^{\circ}\text{E}$ .

Free from the constraint of coastal boundaries, the Kuroshio Extension is known to be an eastward-flowing inertial jet characterized by large-amplitude meanders and energetic pinched-off eddies. Indeed, it was recognized more than two decades ago that the Kuroshio Extension is one of the highest eddy kinetic energy regions in the Pacific Ocean (Wyrтки *et al.*, 1976). Figure 3 shows the eddy kinetic energy (EKE) distributions in the North Pacific based on the first 8-year sea surface height (SSH) data measured by the TOPEX/Poseidon (T/P) satellite altimeters. The top panel (Fig. 3(a)) shows the EKE map calculated from the SSH anomalies after removing signals longer than one year. The EKE thus estimated largely reflects the contributions from the mesoscale eddy signals. Figure 3(a) shows that the highest mesoscale eddy variability occurs between the two quasi-stationary meanders of the Kuroshio Extension. Notice that the high EKE band in Fig. 3(a) extends much further eastward along the mean path of the Kuroshio Extension than that

presented in Wyrтки *et al.* (1976, their figure 4). This discrepancy is likely due to the sparsity of data in the downstream Kuroshio Extension region that were available to Wyrтки *et al.* about 25 years ago.

The high eddy variability has motivated many investigators in the past two decades to examine and quantify the spatial and temporal changes of the Kuroshio Extension. Using water temperature data from XBT measurements, Bernstein and White (1981) and Mizuno and White (1983) investigated the westward propagation of the mesoscale perturbations and the influence of the bathymetric features on the frontal meanders. During the early 1980s, moored current meter measurements were carried out across the Kuroshio Extension along the  $152^{\circ}\text{E}$  and  $165^{\circ}\text{E}$  meridians. From these measurements, Schmitz *et al.* (1982, 1987), Schmitz (1984), and Hall (1989, 1991) carried out extensive analyses of the vertical structure, the frequency distributions, and the energetics of the Kuroshio Extension eddy field.

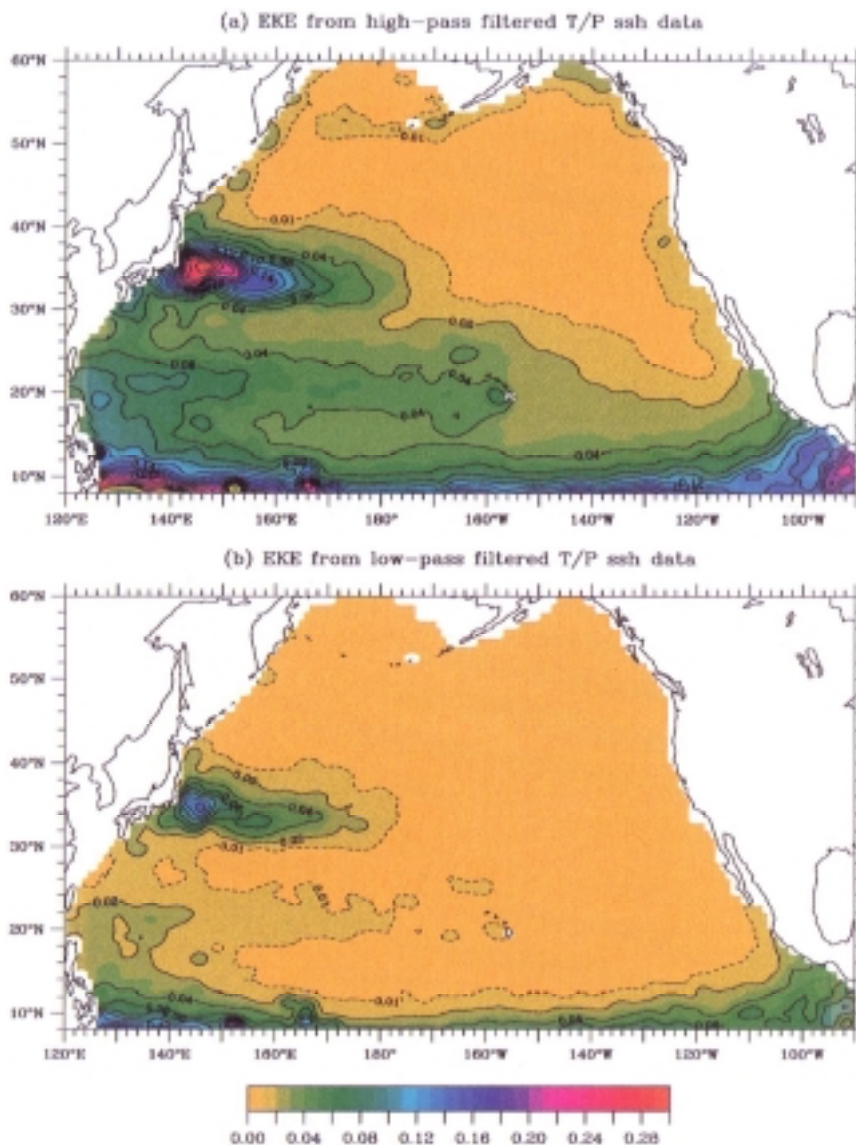


Fig. 3. Eddy kinetic energy (EKE) distributions in the North Pacific Ocean from the T/P SSH data of October 1992 to November 2000. (a) The EKE map based on the SSH anomalies after removing signals longer than the annual period. (b) The EKE map based on the SSH anomalies after removing signals shorter than the annual period. Contour intervals are  $0.02 \text{ m}^2\text{s}^{-2}$  for solid lines; dashed lines denote the  $0.01 \text{ m}^2\text{s}^{-2}$  contours. The EKE values are calculated first along the T/P tracks and are mapped subsequently using a Gaussian smoother with the decorrelation scales of  $1.5^\circ$  long and  $0.75^\circ$  lat.

Many studies of the upstream Kuroshio Extension region near Japan have focused on the mesoscale features, such as warm-core rings, warm tongues, and warm streamers. Using hydrographic data and infrared images of sea surface temperature, Kawai (1972), Kawai and Saitoh (1986), Kawamura *et al.* (1986), Sugimoto *et al.* (1992), and Yasuda *et al.* (1992) described in detail the pinching-off processes of the warm-core rings from the Kuroshio Extension meanders, their interaction with other existing

rings/mesoscale features, and their re-absorption by the meandering Kuroshio Extension. More recently, a number of investigators have examined the roles of the mesoscale fluctuations along the Kuroshio Extension path in facilitating water mass exchanges and transformations between the subtropical and subpolar gyres of the North Pacific Ocean (Talley *et al.*, 1995; Yasuda *et al.*, 1996; Talley, 1997; Yasuda, 1997; Joyce *et al.*, 2001).

The advent of satellite altimetry and the success of

the Geosat and T/P missions have provided great impetus for the study of the mesoscale variability in the Kuroshio Extension region. The studies by Tai and White (1990), Qiu *et al.* (1991), Ichikawa and Imawaki (1994), Aoki *et al.* (1995), Qiu (1995), Mitchell *et al.* (1996), Wang *et al.* (1998), Adamec (1998), Ebuchi and Hanawa (2000), Toba *et al.* (2001), and Tatebe and Yasuda (2001) have made significant progress in the description and understanding of (1) the propagation of mesoscale eddies and meandering disturbances, especially the role played by the advection of the Kuroshio Extension mean flow, (2) the Reynolds stress patterns and the EKE modulations through barotropic conversion processes, and (3) the seasonality of the Kuroshio Extension and its eddy field.

In comparison with the knowledge of mesoscale variability, our understanding of the large-scale, low-frequency variability of the Kuroshio Extension is more limited. By analyzing hydrographic and XBT data from 1976 to 1980, Mizuno and White (1983) showed that the Kuroshio Extension was displaced southward, from 36°–37°N during 1977–78, to 34°N in 1979–80. Associated with this large-scale path change, the quasi-stationary meanders of the Kuroshio Extension became unstable and eddy activity and the ring formation rate increased. Using available temperature measurements from 1950 to 1970, Yamagata *et al.* (1985) showed that, on interannual time scales, the baroclinic transport of the Kuroshio Extension had a lagged, positive correlation with that of the upstream North Equatorial Current. Following individual ENSO events when the NEC transport increased, the Kuroshio Extension tended to intensify 1.5 years later (see also White and He, 1986). By analyzing the altimetry data from the Geosat and ERS-1 missions, Jacobs *et al.* (1994) noted that the Kuroshio Extension path shifted northward in 1992–1993, as compared to 1987–1989. They suggested that this large-scale path shift of the Kuroshio Extension resulted from the passage of a westward-moving warm Rossby wave originating from the 1982/83 equatorial ENSO event.

In this study we first use SSH data from the past 8-year T/P measurements to describe the large-scale changes in the Kuroshio Extension and its southern recirculation gyre (Section 2). One clear outcome of our analysis of the multi-year T/P data is that not only is the Kuroshio Extension the region of the highest mesoscale eddy variability (Fig. 3(a)), it is also where the largest interannual variability is observed in the extratropical North Pacific Ocean (Fig. 3(b)). Possible causes for the observed large-scale changes of the Kuroshio Extension system are explored in Section 3. Specifically, we compare the effect of the internal dynamics of the Kuroshio Extension system with that of the external surface wind forcing. In Section 4 we examine how the observed large-scale changes in the Kuroshio Extension system may impact the

midlatitude ocean-atmosphere coupling by influencing the surface ocean heat budget. The importance of the mode water formation and the re-exposure of the subducted temperature anomalies in the Kuroshio Extension and its neighboring regions is emphasized in Section 5. Section 6 summarizes the issues addressed.

## 2. Large-Scale Variability of the Kuroshio Extension System

As demonstrated in Fig. 3, the Kuroshio Extension region has the highest mesoscale eddy variability in the extratropical North Pacific Ocean. From the viewpoint of wind-driven ocean circulation, this high eddy variability is to be expected. Being a return flow compensating for the wind-driven subtropical interior circulation, the Kuroshio originates at a southern latitude ( $\sim 15^\circ\text{N}$ ) where the ambient potential vorticity (PV) is relatively low. For the Kuroshio to smoothly rejoin the Sverdrup interior flow at the latitude of the Kuroshio Extension, the low PV acquired by the Kuroshio in the south has to be removed by either dissipative or nonlinear forces along its western boundary path. For a narrow boundary current such as the Kuroshio and its extension, scaling analyses show that the dissipative force alone is not sufficient to remove the low PV anomalies (Pedlosky, 1987; Cessi *et al.*, 1990). The consequence of the Kuroshio's inability to effectively diffuse the PV anomalies along its path is the accumulation of the low PV water in the northwestern corner of the subtropical gyre, which generates a mean anticyclonic recirculation gyre and provides an energy source for flow instability (Qiu and Miao, 2000).

That the recirculation gyre is an inseparable part of the Kuroshio Extension system is well demonstrated by lowered ADCP measurements from a recent WOCE cruise across the Kuroshio Extension southeast of Japan (see line P10 in Fig. 4). Figure 5 shows the surface-to-bottom profile of the northeastward velocity from this cruise. The volume transport of the eastward-flowing Kuroshio Extension, denoted in Fig. 5 by the unshaded area, is about 140 Sv (Wijffels *et al.*, 1998). This is three times as large as the maximum Sverdrup transport of about 45 Sv in the subtropical North Pacific (Fig. 4; see also Hautala *et al.*, 1994; Huang and Qiu, 1994). The inflated eastward transport is due to the presence of the westward recirculating flow south of the Kuroshio Extension. Though weak in its surface speed, the lowered ADCP measurements show that this westward recirculating flow has a strong *barotropic* component and has a total volume transport exceeding 90 Sv (Wijffels *et al.*, 1998; their figure 6). Notice that the *net* eastward transport of the Kuroshio Extension across the P10 line is  $\sim 50$  Sv and is close to the maximum Sverdrup transport value of the North Pacific subtropical gyre. Another important feature revealed in Fig. 5 is the non-existence of the so-called “level of no

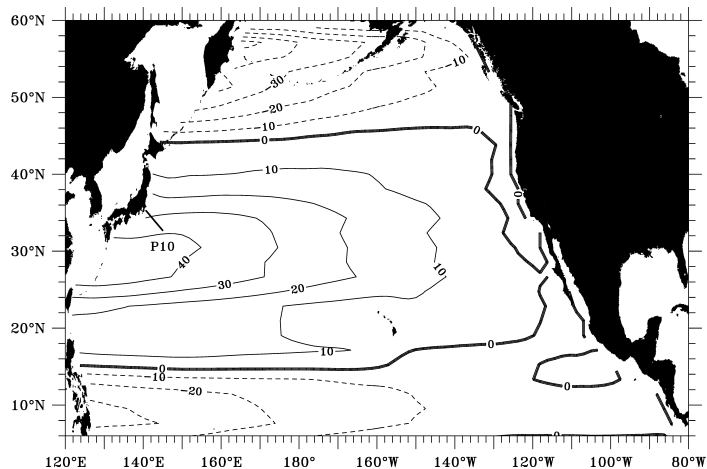


Fig. 4. Sverdrup transport streamfunction calculated from the 1980–1999 mean surface wind stress data of NCEP/NCAR reanalysis (Kalnay *et al.*, 1996). Units in Sv.

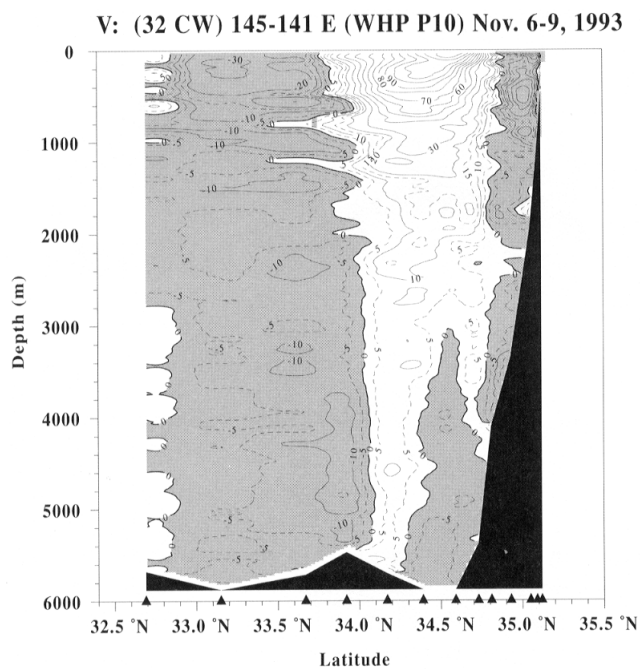


Fig. 5. Northeastward velocity profile from lowered acoustic Doppler current meter profiler (ADCP) measurements along the WOCE P10 line southeast of Japan in November 1993 (see the dark line in Fig. 4 for its location). Units are  $\text{cm s}^{-1}$  and southwestward flow is shaded. Figure courtesy of Drs. E. Firing and P. Hacker of University of Hawaii.

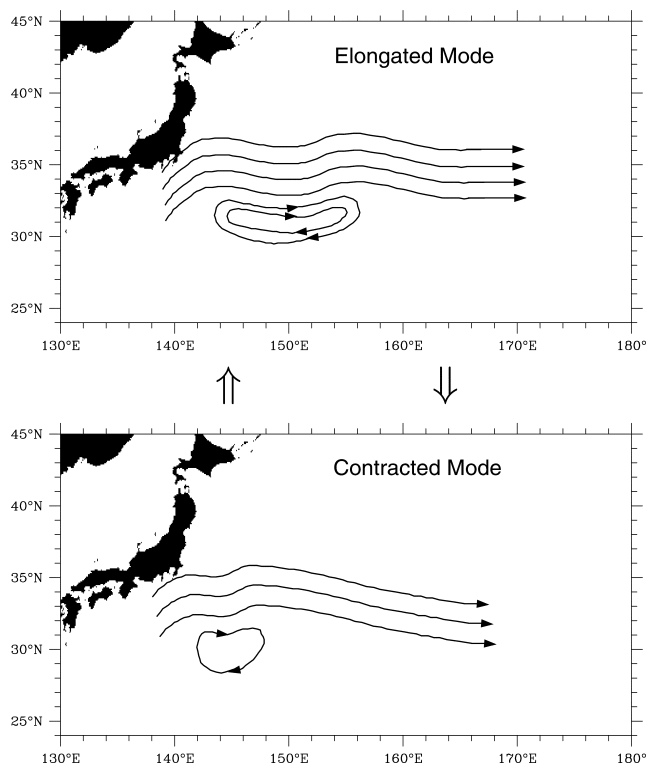


Fig. 6. Schematic of the large-scale oscillating patterns of the Kuroshio Extension system. In the elongated mode, the Kuroshio Extension has a stronger eastward surface transport, a more northerly mean position, and an intensified southern recirculation gyre. In the contracted mode, the Kuroshio Extension has a weaker eastward surface transport, a more southerly mean position, and a less intense southern recirculation gyre.

motion". A transport estimation by assuming a level of no-motion, even at a depth greater than 2,000 dbar, would significantly underestimate the transport values for *both* the eastward-flowing Kuroshio Extension and the west-

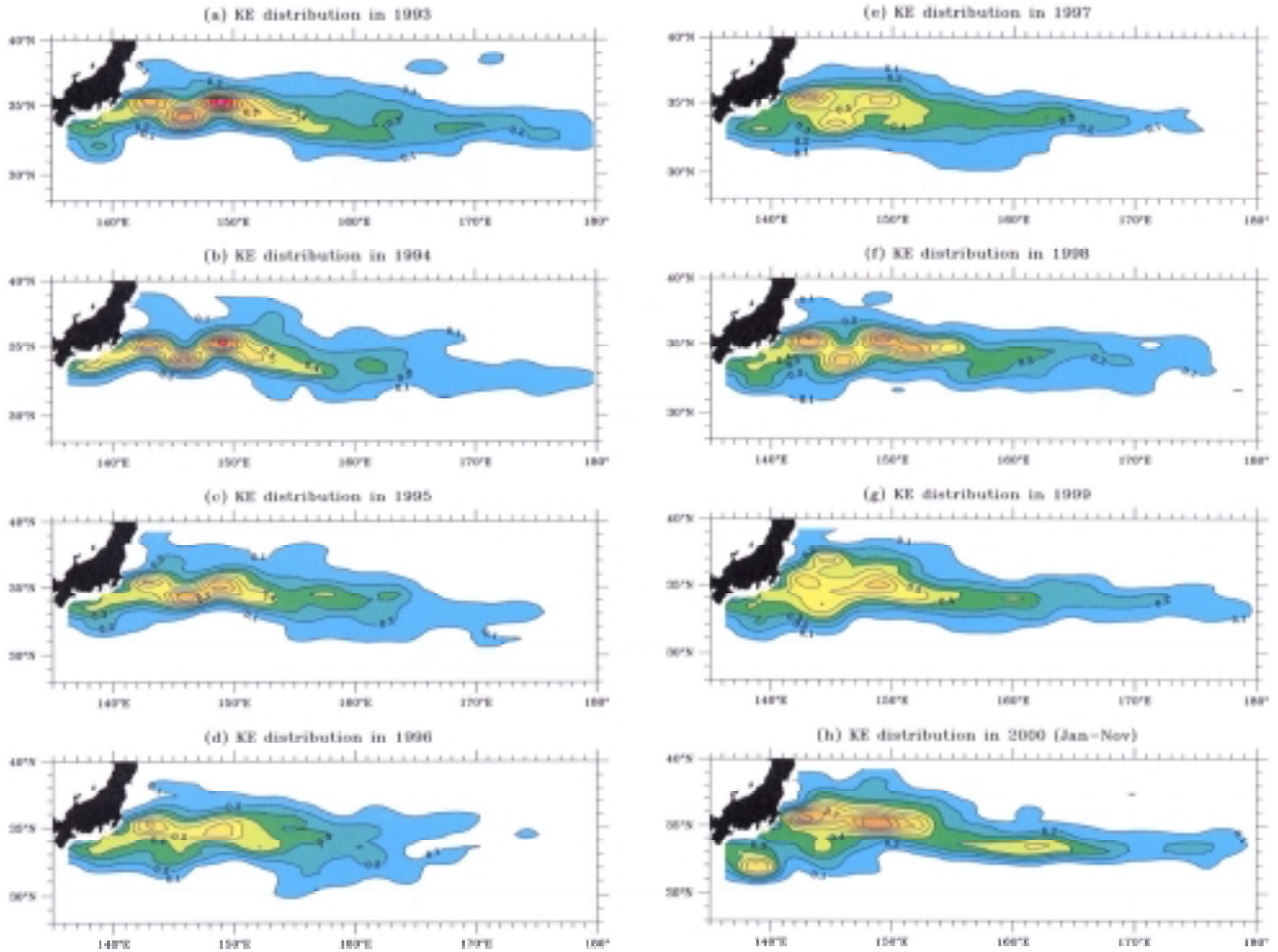


Fig. 7. Yearly-averaged total kinetic energy distributions estimated from the along-track absolute SSH data. Contour intervals are  $0.1 \text{ m}^2\text{s}^{-2}$ .

ward-flowing recirculation. From these in-situ observations, it is clear that if we are to understand the large-scale Kuroshio Extension variability, we need to clarify the recirculating component of the Kuroshio Extension system.

From the T/P measurements, the large-scale changes of the Kuroshio Extension system over the past 8 years can be succinctly summarized as in Fig. 6. From late 1992 to 1996, the Kuroshio Extension evolved gradually from an elongated state to a contracted one. This modal transition reversed after 1997 and the Kuroshio Extension returned to the elongated state in 1999 and 2000. As depicted schematically in Fig. 6, in the elongated state, the Kuroshio Extension has a larger eastward surface transport, a greater zonal penetration, and a more northerly zonal-mean path. All these characteristics are closely connected to the presence of an intense, zonally-elongated

southern recirculation gyre. In its contracted state, the Kuroshio Extension has a smaller eastward surface transport, a more southerly mean path, and is accompanied by a weaker southern recirculation gyre.

The oscillation of the Kuroshio Extension system between the elongated and contracted states can be demonstrated in several ways. Figure 7 shows the yearly-averaged kinetic energy distributions in the Kuroshio Extension region. Here, the kinetic energy (KE) is estimated from the along-track SSH (anomaly + mean; the mean SSH field is shown in Fig. 2) data by assuming geostrophy and isotropic conditions. Since the KE level closely reflects the Kuroshio Extension jet, the high KE band that can be seen to extend beyond the dateline in 1993 (Fig. 7(a)) indicates the zonally elongated state of the Kuroshio Extension system. The high KE band retracts steadily in subsequent years, reaching a zonal minimum in 1996.

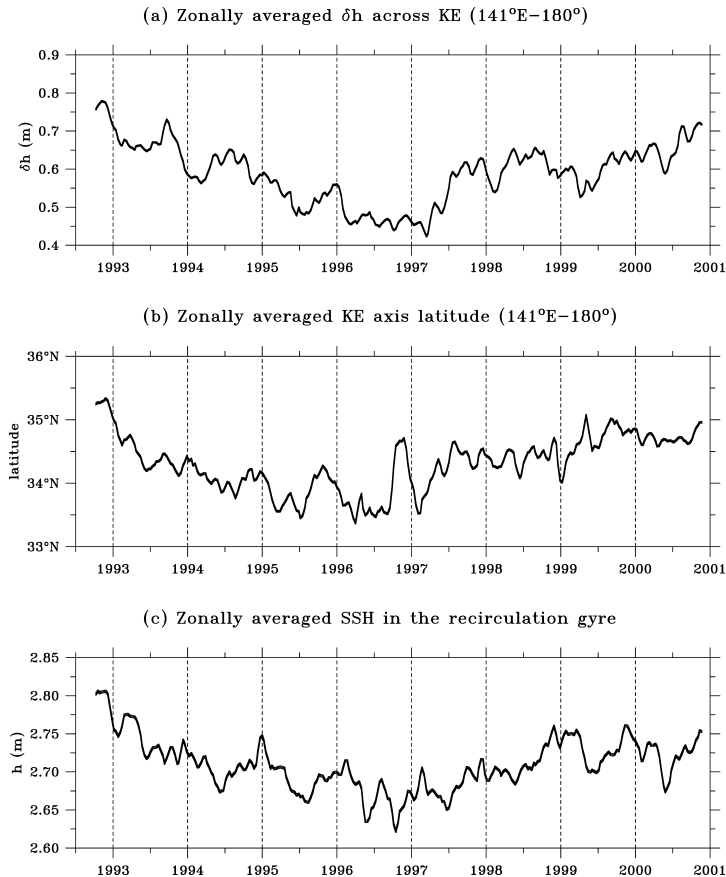


Fig. 8. Time series of (a) the zonally averaged SSH difference across the Kuroshio Extension, (b) the zonally averaged axis position of the Kuroshio Extension, and (c) the zonally averaged SSH in the recirculation gyre. Here, the zonal average is from 141°E to 180°.

Following 1997, the trend is reversed and a gradual eastward expansion of the high KE band is evident in Figs. 7(e)–(h).

Figure 8 shows the times series of (a) the zonally-averaged SSH difference ( $\delta h$ ) across the eastward-flowing Kuroshio Extension, (b) the zonally-averaged position of the Kuroshio Extension jet, and (c) the zonally-averaged SSH ( $h_R$ ) in the Kuroshio Extension recirculation gyre. Here,  $\delta h$  is evaluated along individual T/P tracks by identifying the center of the Kuroshio Extension jet (where the eastward surface flow is maximum), averaging the SSH values over a 1°-bin 1.5 degrees north and south of the jet's center ( $h_N$  and  $h_S$ ), and taking the difference,  $h_S - h_N$ . For  $h_R$ , the SSH is averaged from 28°N to the southern edge of the Kuroshio Extension jet (defined at 2° south of the jet's center). All zonal averages in Fig. 8 are taken from 141°E to 180°. The interannual signal in the three time series is similar: during the elongated state before 1993 and after 1999, the Kuroshio Extension has a stronger eastward surface transport, a more northerly mean position, and an intensified southern recirculation

gyre. During the contracted state around 1996, the Kuroshio Extension has a weaker eastward surface transport, a more southerly mean position, and a less intense southern recirculation gyre.

Finally, the two contrasting modes of the Kuroshio Extension system may be verified by simply inspecting the observed SSH maps. Figure 9 shows the SSH maps for November of 1992, 1995, and 1999. The Kuroshio Extension is in the elongated mode in 1992 and 1999, and in the contracted mode in 1995. Many of the characteristics that distinguish the two modes, such as the zonal penetration of the Kuroshio Extension jet and the intensity of the recirculation gyre, can be visually confirmed in these SSH maps.

### 3. Possible Causes of the Bimodal Kuroshio Extension Changes

Given the results of the preceding section, it is natural to ask the causes of the observed bimodal changes in the Kuroshio Extension system. Dynamically, there are at least two possibilities: (a) that the bimodal fluctuations

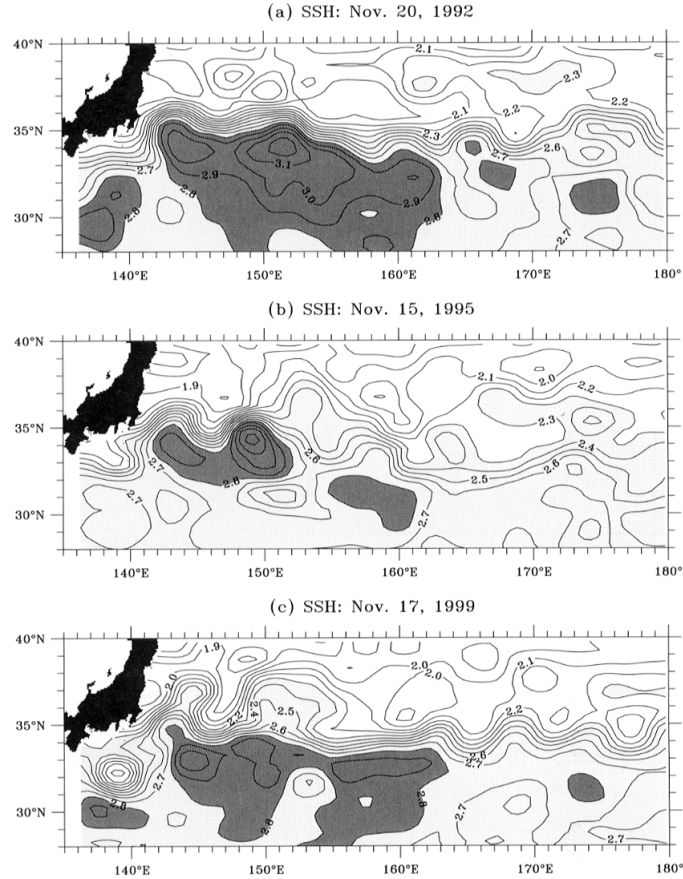


Fig. 9. Sea surface height fields on (a) 20 November 1992, (b) 15 November 1995, and (c) 17 November 1999.

are a consequence of the internal nonlinear dynamics of the Kuroshio Extension system, and (b) that they are externally induced by interannual-to-decadal changes in the basin-wide wind stress curl field. We explore these two possibilities in turn in this section.

The presence of the intense southern recirculation gyre (recall Fig. 5) clearly signifies that the Kuroshio Extension system is highly nonlinear. For highly nonlinear western boundary current (WBC) outflow systems, the low-frequency variability caused by transitions between multiple equilibrium states has been the subject of several recent studies (e.g., Jiang *et al.*, 1995; McCalpin and Haidvogel, 1996; Spall, 1996; Berloff and McWilliams, 1999; Qiu and Miao, 2000). Of particular interest to this study is that of McCalpin and Haidvogel (1996), in which they used a reduced-gravity, quasi-geostrophic model driven by the *steady*, classical double-gyre wind forcing. In the parameter range where the wind-driven circulation system is weakly unstable, McCalpin and Haidvogel found the existence of multiple WBC patterns that are distinguished by their energy levels and outflow jet shapes. The “high-energy” pattern, which resembles the

elongated mode of the Kuroshio Extension depicted in Fig. 6, has an elongated eastward penetration of the WBC outflow, which meanders moderately. The “low-energy” pattern, similar to the contracted mode of Fig. 6, is characterized by violent meandering and eddy formation in the upstream region of the WBC outflow. During this state, the existence of the eastward penetrating jet is not always obvious. With regard to the dynamics governing these two patterns, McCalpin and Haidvogel found that the eddy-jet interaction works to damp the jet meanders during the “high-energy” state, whereas it enhances the jet meanders and eddy generation during the “low-energy” state.

The absence of broad-scale, synoptic measurements of subsurface thermal structures in the Kuroshio Extension region prevents us from evaluating directly the eddy-jet interaction in the two contrasting states of the Kuroshio Extension system. Nevertheless, by considering the observed eddy kinetic energy (EKE) changes as manifestations of eddy-jet interaction, we can compare the observations with McCalpin and Haidvogel’s (1996) work as a consistency check. Notice that in the McCalpin and Haidvogel paper (their figure 5), the EKE level in the

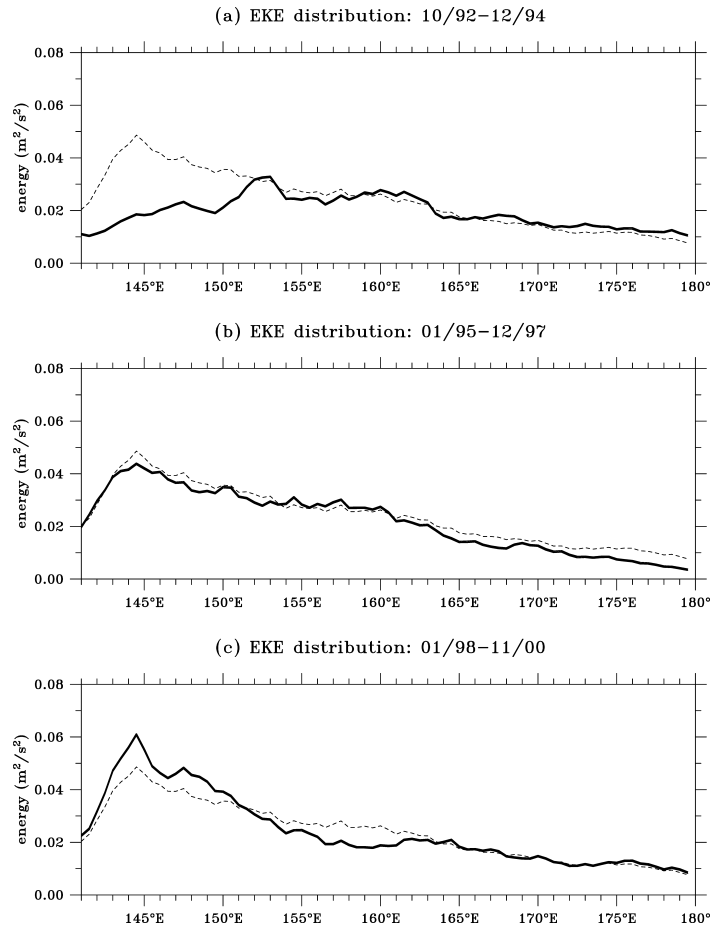


Fig. 10. Eddy kinetic energy distributions (solid lines) as a function of longitude averaged in a  $6^\circ$ -wide band along the Kuroshio Extension path: (a) November 1992–December 1994, (b) January 1995–December 1997, and (c) January 1998–November 2000. Dashed lines denote the EKE distributions over the entire T/P period from November 1992 to November 2000.

upstream WBC outflow region is low during the “high-energy” state and high during the “low-energy” state.

Figure 10 shows the longitudinal distributions of the observed EKE during the three periods: (a) November 1992–December 1994, (b) January 1995–December 1997, and (c) January 1998–November 2000. Here, the EKE value has been meridionally averaged over a  $6^\circ$  band along the observed path of the Kuroshio Extension jet. Comparing Figs. 10(a) with 10(b) shows that the EKE level in the upstream Kuroshio Extension region from  $141^\circ\text{E}$  to  $155^\circ\text{E}$  was higher when the Kuroshio Extension was in the contracted mode (Period (b)) than in the elongated mode (Period (a)). This is consistent with McCalpin and Haidvogel’s result that the eddy-jet interaction during the contracted state of the WBC system enhances the eddy activity in the upstream WBC outflow region. When the Kuroshio Extension returned back to the elongated state after 1998, however, Fig. 10(c) shows that the EKE level in the upstream Kuroshio Extension did *not* decrease as

would be expected from the McCalpin and Haidvogel study. In other words, the observational results shown in Fig. 10 are inconclusive as to whether the McCalpin and Haidvogel (1996) mechanism is at work for the observed bimodal changes in the Kuroshio Extension system.

Being the WBC outflow that compensates for the wind-driven interior Sverdrup flow, the Kuroshio Extension will be affected by the wind stress curl fluctuations over the subtropical North Pacific Ocean. Indeed, several investigators have demonstrated that decadal variations in the basin-wide wind stress curl field of the subtropical North Pacific are responsible for the observed transport changes in the Kuroshio (Qiu and Joyce, 1992; Akitomo *et al.*, 1996) and the Kuroshio Extension (Yasuda and Hanawa, 1997; Miller *et al.*, 1998; Deser *et al.*, 1999; Xie *et al.*, 2000). For the upstream Kuroshio Extension in particular, Deser *et al.* (1999) showed that the depth-averaged geostrophic transport change of the Kuroshio Extension between the decades of 1970–1980 and 1982–

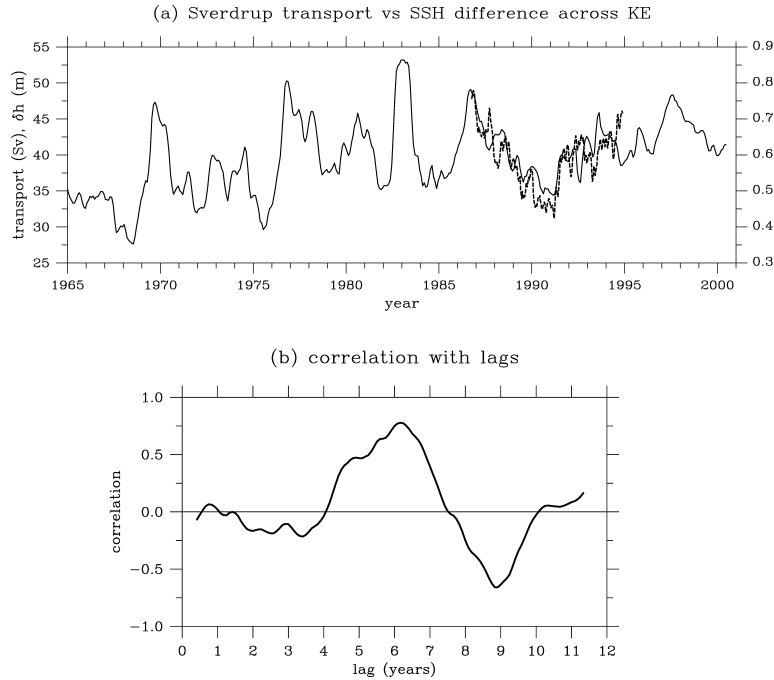


Fig. 11. (a) Solid line: Sverdrup transport time series in the latitude band between 29°N and 32°N calculated from the monthly wind stress curl data of NCEP/NCAR reanalysis (Kalnay *et al.*, 1996). Variability shorter than the annual period has been removed. Dashed line: zonally averaged SSH difference across the Kuroshio Extension; same as in Fig. 8(a), except it is plotted with a lag of 6 years. (b) Correlation coefficient between the time series of the Sverdrup transport and that of the zonally-averaged SSH difference across the Kuroshio Extension with various time lags.

1990 (11.6 Sv) can be *quantitatively* accounted for by the Sverdrup transport change between the decades of 1968–1976 and 1977–1988 (11.5–13.9 Sv). Notice that most of the aforementioned studies have considered the connection between the changes in the interior Sverdrup transport and the Kuroshio/Kuroshio Extension from the viewpoint of mass conservation. For the reasons stated in Section 2, it is conceivable that as the wind-driven Sverdrup transport increases, the enhanced WBC could carry additional low-PV water into the Kuroshio Extension region, intensifying the southern inertial recirculation gyre and augmenting the transport of the eastward-flowing Kuroshio Extension.

With the availability of the detailed T/P measurements, it is of interest to re-examine the relationship between the large-scale changes in the Kuroshio Extension and those in the basin-wide wind stress curl field. The solid line in Fig. 11(a) shows the time series of the Sverdrup transport in the latitude band of 29°N–32°N (as shown in Fig. 4, this latitude band gives the maximum Sverdrup transport value in the North Pacific subtropical gyre). As noted in many previous studies, interannual-to-decadal time scale changes in the subtropical North Pacific Sverdrup transport are abundant. To compare these changes with the observed Kuroshio Extension variabil-

ity, we computed the correlation coefficient between this time series and that of the zonally-averaged SSH difference ( $\delta h$ ) across the Kuroshio Extension (i.e., Fig. 8(a)) at different time lags. As shown in Fig. 11(b), the maximum correlation,  $r = 0.78$ , is found when the surface transport of the Kuroshio Extension\* lags the Sverdrup transport by about 6 years. (For comparison, the  $\delta h$  time series with a lag of 6 years is plotted in Fig. 11(a) as the dashed line.) It is interesting to note that the 6-year value is very close to the lags of 4–6 years found by Miller *et al.* (1998), Deser *et al.* (1999), and Schneider and Miller (2001). In these three studies, the authors have used different methods, including composite data analysis and ocean modeling, to evaluate the lag between the decadal changes in the basin-wide wind stress curl field and the Kuroshio Extension. Physically, the 6-year lag denotes the adjustment time needed by baroclinic Rossby waves to transit from the central North Pacific, where the decadal wind stress curl variability is at a maximum, to the western boundary along the Kuroshio Extension latitudes (Deser *et al.*, 1999).

\*The surface transport of the Kuroshio Extension,  $T$ , is linearly related to the SSH difference by  $T = g\delta h/f$ , where  $g = 9.8 \text{ m s}^{-2}$  and  $f = 8.34 \times 10^{-5} \text{ s}^{-1}$ .

Because the T/P-derived SSH difference only provides a measure for the surface transport of the Kuroshio Extension, a quantitative comparison between the two time series in Fig. 11(a) requires converting the  $\delta h$  time series to the *volume transport* of the Kuroshio Extension. Direct current measurements and repeat hydrographic surveys were carried out by Imawaki *et al.* (2001) along a T/P ground track near 133°E across the Kuroshio south of Japan. From the concurrent in-situ and T/P measurements, Imawaki *et al.* found a tight relationship between the volume transport of the eastward-flowing Kuroshio and the T/P-measured SSH difference across the Kuroshio. Specifically, a 0.5 m change in  $\delta h$  is found to correspond to a 40 Sv change in the volume transport of the Kuroshio (see figure 2 in Imawaki *et al.*, 2001). In Fig. 11(a), the correspondence between  $\delta h$  and the Sverdrup transport change is 0.5 m vs. 25 Sv. If we assume that the conversion rate derived for the Kuroshio south of Japan is valid in the Kuroshio Extension region, the result of Fig. 11(a) implies that for a 40 Sv volume transport change (manifested as a 0.5 m change in  $\delta h$ ) in the Kuroshio Extension, 25 Sv would be related to the interior Sverdrup transport and the remaining 15 Sv has to result from the changes in the inertial recirculation gyre. The fact that the intensity of the observed recirculation gyre does change in phase with the  $\delta h$  time series (see Fig. 8(c)) lends support to this hypothesis. As we noted above, this is also consistent with the notion that as the Sverdrup transport increases, the additional low-PV water carried northward into the Kuroshio Extension region can intensify the inertial recirculation gyre and inflate the transport change in the eastward-flowing Kuroshio Extension.

#### 4. Midlatitude Ocean-Atmosphere Coupling

The Kuroshio Extension system resides in the region where the North Pacific Ocean loses large quantities of its heat to the overlying atmosphere. This large heat loss, with the wintertime net heat flux value exceeding  $-450 \text{ W m}^{-2}$  (Fig. 12(a)), results from the cold, dry air from the Eurasian continent overriding the warm waters transported poleward by the Kuroshio and its extension. Notice that averaged annually, the net heat flux from the ocean to the atmosphere over the Kuroshio Extension region ranges from  $-50$  to  $-150 \text{ W m}^{-2}$  (Fig. 12(b)). In order to maintain the thermodynamic equilibrium in the surface ocean and the atmospheric boundary layer, this net heat loss must be balanced by heat advection of the *ocean circulation*. The preferred paths of wintertime extratropical storms also lie over the area where the heat loss from the ocean to the atmosphere is largest. Because these storms are commonly accompanied by excessive rainfall, their tracks can be identified in the wintertime precipitation climatology as regions of high precipitation (Fig. 12(c)). As with the wintertime net heat flux climatology, the maxi-

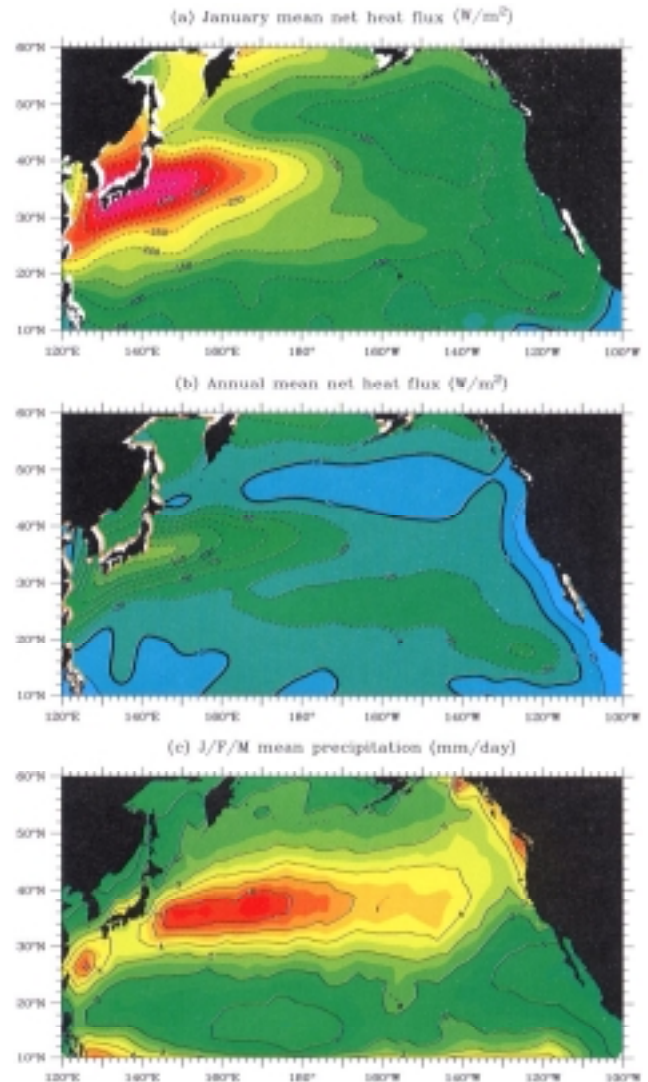


Fig. 12. (a) January mean net heat flux over the North Pacific Ocean. Based on Da Silva *et al.* (1994). (b) Same as (a) except for the annual mean. (c) Wintertime (J/F/M) mean precipitation over the North Pacific Ocean. Based on Xie and Arkin (1997).

imum J/F/M precipitation occurs in the latitude band of 34°N–40°N, that parallels the eastward-flowing Kuroshio Extension (cf. Fig. 2). Given the proximity of the areas of the maximum air-sea heat exchange, the atmospheric storm tracks, and the maximum low-frequency oceanic variability (recall Fig. 3(b)), it is conceivable that the large-scale fluctuations occurring in the Kuroshio Extension system could change the upper ocean heat balance and modify the atmospheric circulation at long time scales by altering the baroclinicity and positions of the wintertime storms.

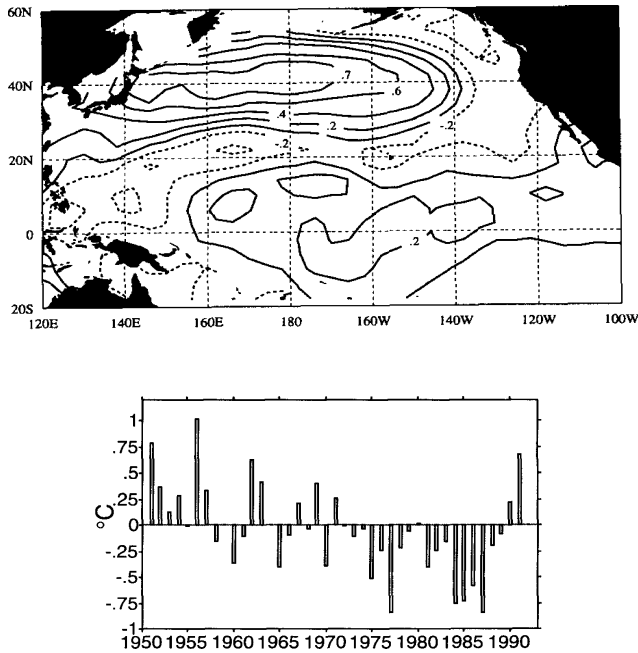


Fig. 13. Top panel: Spatial pattern of the second EOF mode of the wintertime SST anomalies (1950–1992) in the Pacific Ocean. This mode explains 11% of the variance over the domain. Bottom panel: Time series of the wintertime SST anomalies averaged in the Kuroshio-Oyashio outflow region ( $32^{\circ}\text{N}$ – $46^{\circ}\text{N}$ ,  $136^{\circ}\text{E}$ – $176^{\circ}\text{W}$ ). Adapted from Deser and Blackmon (1995).

The ocean influences the atmospheric circulation on the interannual-to-decadal time scales through anomalies of sea surface temperature (SST). In the past decade, many investigators have examined low-frequency SST changes in the Pacific Ocean (e.g., Tanimoto *et al.*, 1993; Miller *et al.*, 1994; Deser and Blackmon, 1995; Mantua *et al.*, 1997; Nakamura *et al.*, 1997; Zhang *et al.*, 1997). Note that all of these studies have focused on the wintertime signals because winter is the season when the midlatitude ocean-atmosphere interaction is most active. A common finding from these studies is the existence of a distinct SST mode with a decadal time scale in the midlatitude North Pacific. As shown in Fig. 13 (adapted from Deser and Blackmon, 1995), the center of action of this decadal SST mode is in the Kuroshio Extension and Oyashio confluence region; the temporal characteristics of this mode, Fig. 13, have been shown by Nakamura *et al.* (1997) to be independent of the decadal tropical ENSO signals.

The decadal SST signal shown in Fig. 13 is one manifestation of the Pacific decadal oscillation (PDO) and its causes have been the subject of many recent diagnostic and coupled modeling studies. One of the primary candidate mechanisms hypothesized for the PDO involves the

North Pacific subtropical ocean circulation interacting with the Aleutian Low atmospheric pressure system. Using a coupled general circulation model, Latif and Barnett (1994, 1996) show that an enhanced meridional SST gradient in their modeled WBC outflow region tends to strengthen the overlying westerlies and intensify the basin-scale wind stress curl field. As the WBC responds to this changing wind stress curl field, its heat advection works to reverse the sign of the original SST anomaly gradient in the WBC outflow region, causing oscillations of the coupled ocean-atmosphere system with a period of about 20 years. Notice that there are three components involved in the Latif and Barnett feedback mechanism:

1. oceanic adjustment to the changing wind stress curl field,
2. SST response in the WBC outflow region to the changing WBC, and
3. atmospheric response to the changing SST gradient pattern.

In the following, we focus on the oceanic processes that are relevant to component (2).

Figure 14(a) shows the zonally-averaged wintertime (J/F/M) SST anomalies as a function of year and latitude. Here, the SST data are based on the NCEP reanalysis and the zonal average is taken from  $142^{\circ}\text{E}$  to  $180^{\circ}$ . As plotted in Fig. 14(b), the decadal SST signals along the Subarctic Frontal Zone of  $40^{\circ}\text{N}$ – $44^{\circ}\text{N}$ , such as the warming in 1950–1957 and cooling in 1975–1989, are consistent with the SST anomaly signals presented in Fig. 13. For comparison, we also plot in Fig. 14(b) the SST anomalies in the Kuroshio Extension band ( $32^{\circ}\text{N}$ – $36^{\circ}\text{N}$ ). As shown in Fig. 12(c), the bands of the Subarctic Frontal Zone and the Kuroshio Extension straddle the midlatitude wintertime storm tracks. Although the highest SST variance is observed along the Subarctic Frontal Zone (Nakamura and Kazmin, 2001), it is interesting to note from Fig. 14(a) that the SST anomalies in the subtropical gyre often precede those in the Subarctic Frontal Zone. One consequence of this difference between the SST anomalies across the subtropical and subpolar gyre boundary is that the meridional SST difference  $T'_{SF} - T'_{KE}$ , to which the wintertime storm tracks are likely to be sensitive, has a time series that is subtly different from either the  $T'_{SF}$  or  $T'_{KE}$  time series (see Fig. 14(b)). As such, understanding the component (2) of the Latif and Barnett feedback mechanism requires clarifying the anomalous SST signals in the bands along *both* the Kuroshio Extension and the Subarctic Frontal Zone.

A useful approach to studying the SST changes is to consider the heat balance in the surface ocean mixed layer. As discussed by Qiu and Kelly (1993), the equation governing the mixed layer temperature  $T_m$ , which is a good proxy for SST in winter, can be written as:

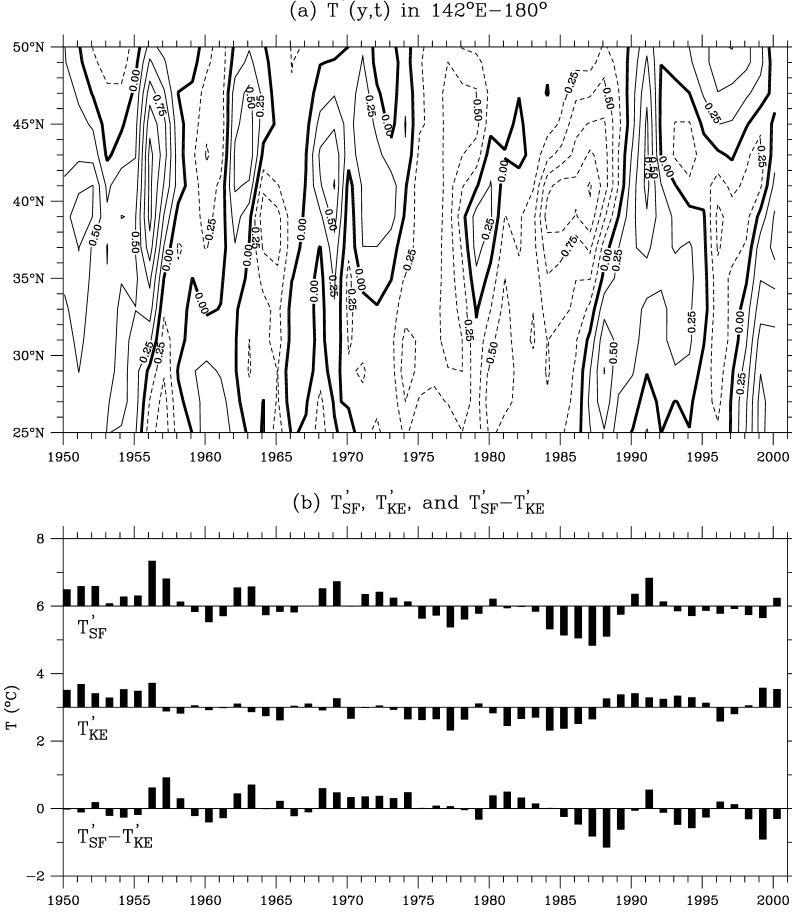


Fig. 14. (a) Wintertime (J/F/M) SST anomalies as a function of year and latitude. Based on the NCAR/NCEP reanalysis data (Kalnay *et al.*, 1996). (b) J/F/M SST anomalies in the Subarctic Frontal Zone of  $40^\circ\text{N}-44^\circ\text{N}$  ( $T'_{SF}$ ), the Kuroshio Extension  $32^\circ\text{N}-36^\circ\text{N}$  ( $T'_{KE}$ ), and their difference. Here, all SST anomalies are zonally averaged from  $142^\circ\text{E}$  to  $180^\circ$ .

$$\frac{\partial T_m}{\partial t} = \frac{Q_{net}}{\rho_o c_p h_m} - \mathbf{u}_e \cdot \nabla T_m - \frac{w_e (T_m - T_d)}{h_m} - \mathbf{u}_g \cdot \nabla T_m, \quad (1)$$

where  $Q_{net}$  denotes the net surface heat flux,  $\rho_o$  and  $c_p$  are the reference density and specific heat of seawater, respectively,  $h_m$  is the mixed layer depth,  $\mathbf{u}_e$  is the Ekman velocity and is related to the surface wind stress vector  $\boldsymbol{\tau}$  by  $\mathbf{u}_e = \boldsymbol{\tau} \times \mathbf{k} / \rho_o f h_m$ ,  $w_e$  is the entrainment velocity,  $T_d$  is the water temperature below the base of the mixed layer, and  $\mathbf{u}_g$  is the surface geostrophic velocity and is related to the SSH  $h$  by  $\mathbf{u}_g = g \mathbf{k} \times \nabla h / f$ .

It is worth mentioning that although anomalous surface heat flux forcing has been considered to be the dominant contributor to non-seasonal SST anomalies in midlatitudes (e.g., Davis, 1976; Frankignoul, 1985), more recent studies by Cayan (1992) and Iwasaka and Wallace (1995) have found that the time rates of change of SST anomalies and the anomalous surface heat fluxes are not highly correlated in the WBC outflow region of the North

Pacific. As shown in Fig. 15 (adapted from Iwasaka and Wallace, 1995), a typical correlation coefficient in the WBC outflow region is about  $-0.4$  (in contrast to  $-0.6$  in the central and eastern North Pacific), suggesting the importance of the WBC variability in influencing the regional, non-seasonal SST changes. A careful look at the wintertime SST anomalies in the Kuroshio Extension region in Fig. 14(b) reveals that  $T'_{KE}$  was positive in 1993–1995, negative in 1996/1997, and positive again in 1998–2000. This interannual signal of  $T'_{KE}$  seems to correspond to the interannual signal of the Kuroshio Extension system described in Section 2, namely, warm (cold) wintertime SST anomalies tend to appear when the Kuroshio Extension system is in an elongated (contracted) state (cf. Fig. 8).

In order to quantify the relative contributions of various physical processes to the observed SST changes in the Kuroshio Extension region, Qiu (2000) evaluated the individual terms in Eq. (1) by combining available data from the NCAR/NCEP reanalysis, the upper ocean ther-

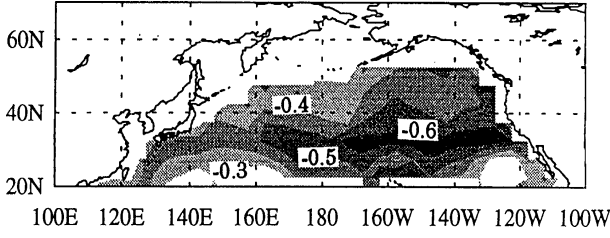


Fig. 15. Correlation coefficient between the nonseasonal wintertime (DJFM) surface heat flux and the nonseasonal wintertime SST tendency. Based on the Comprehensive Ocean-Atmosphere Data Set (COADS) of 1950–1986. Adapted from Iwasaka and Wallace (1995).

mal data set of White (1995), and the T/P SSH measurements. Because the T/P SSH data are available only after October 1992, a full analysis of Eq. (1) was restricted to the winters (J/F/M) of 1993 to 1999. Figure 16(a) shows the time series of the nonseasonal temperature tendency term averaged in the Kuroshio Extension region ( $31^{\circ}\text{N}$ – $37^{\circ}\text{N}$ ,  $141^{\circ}\text{E}$ – $180^{\circ}$ ). For comparison, the sum of nonseasonal surface heat flux forcing, Ekman advection, and vertical entrainment is shown in Fig. 16(b). These three terms have traditionally been included in the “one-dimensional” modeling of the surface ocean mixed layer, and their sum in the wintertime Kuroshio Extension region is dominated by the nonseasonal surface heat flux forcing term,  $(Q_{net}/\rho_0 c_p h_m)'$ . The correlation coefficient between the time series in Figs. 16(a) and (b) is only 0.38, which is similar to the 0.43 value found by Iwasaka and Wallace (1995) as shown in Fig. 15.

Figure 16(c) shows the nonseasonal geostrophic advection term,  $-(\mathbf{u}_g \cdot \nabla T_m)'$ . Reflecting the interannual changes in the Kuroshio Extension system, this term works to lower  $T'_m$  in 1993–1995 when the Kuroshio Extension system changed from an elongated state to a contracted state, and to increase  $T'_m$  in more recent years when the Kuroshio Extension system returned from the contracted state to an elongated state. Notice that adding the nonseasonal geostrophic advection to the “one-dimensional” mixed layer processes (Fig. 16(d)) increases the correlation coefficient with the nonseasonal temperature tendency term (Fig. 16(a)) to 0.80. This improved correlation underlines the importance of heat advection by the surface ocean circulation in determining the wintertime SST anomaly signals in the Kuroshio Extension region. A visual comparison between Figs. 16(a) and (d) indicates that the time series in Fig. 16(d) tends to overestimate the amplitude of the observed  $(\partial T_m / \partial t)'$  term. This discrepancy could be due to the fact that meso-scale eddy heat fluxes, which are important in the Kuroshio Extension region (e.g., Wunsch, 1999), were not included in Eq. (1).

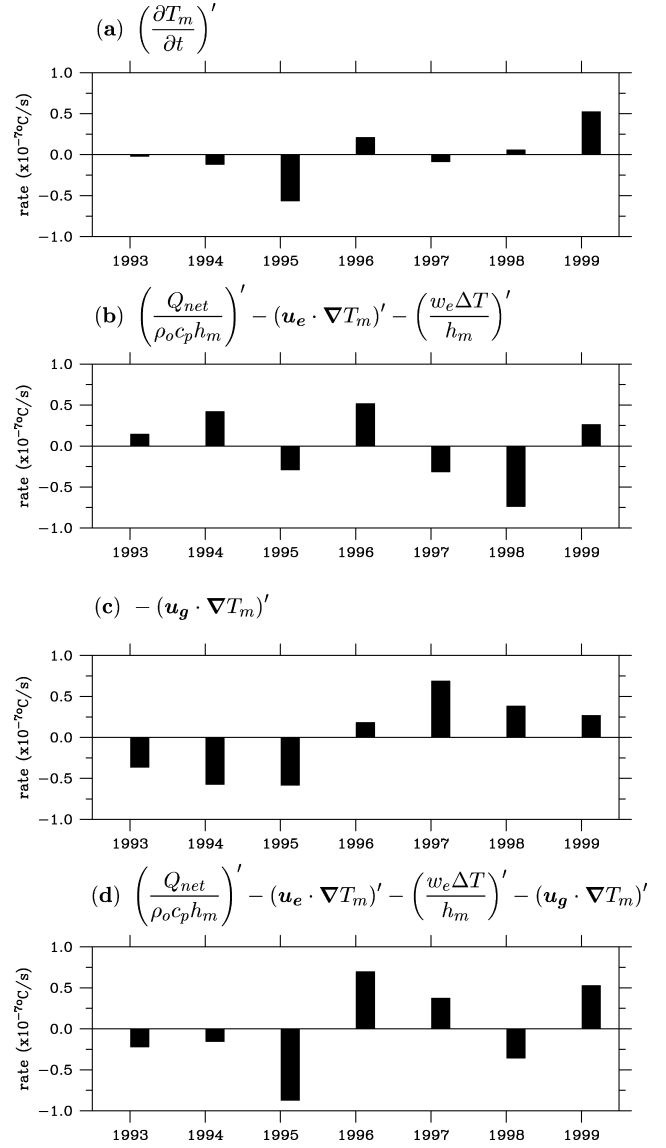


Fig. 16. Time series of terms in the surface ocean heat budget equation (1). All values have been averaged in the Kuroshio Extension region of  $31^{\circ}\text{N}$ – $37^{\circ}\text{N}$  and  $141^{\circ}\text{E}$ – $180^{\circ}$  and  $a'$  denotes the wintertime (J/F/M) anomaly of the term  $a$  from its seasonal mean value. Adapted from Qiu (2000).

A surface ocean heat budget study for the Kuroshio Extension region was also carried out recently by Yasuda *et al.* (2000). In their study, Yasuda *et al.* analyzed the SST anomaly signals of 1955–1992 and regarded the geostrophic advection effect as the residue of the remaining four terms in Eq. (1). One important result from their study is that the geostrophic advection not only contributes to the non-seasonal SST anomalies through horizontal heat convergence/divergence, it also modifies the surface ocean heat budget by changing the mixed layer depth,

$h_m$ . Three years prior to the cold-to-warm transition in SST anomalies in the Kuroshio Extension region in 1987/1988 (see  $T'_{KE}$  in Fig. 14(b)), Yasuda *et al.* found that  $h_m$  changed from a deep to a shallow phase. They argued that this shoaling in the mixed layer depth due to horizontal flow divergence in 1985 contributed to the warming in  $T'_{KE}$  three years later.

## 5. STMW and Obduction

It is worth emphasizing that the Kuroshio Extension and the Subarctic Frontal Zone are regions where ocean dynamics and thermodynamics are intimately connected. As shown in Fig. 17(a), the southern recirculation of the Kuroshio Extension is where intense subduction occurs that transfers cold surface water of late winter into the underlying thermocline and forms the Subtropical Mode Water (STMW; for an excellent review of mode waters, see Hanawa and Talley, 2001). Notice that in the Kuroshio Extension recirculation, STMW, characterized by a thermostat or a low-PV layer, is observed to have a core depth at 250 m and a vertical thickness of 200 m (Suga *et al.*, 1997). Since the maximum wintertime mixed layer depths in this region are no greater than 175 m (Huang and Qiu, 1994; Suga *et al.*, 1997), STMW should be interpreted as existing in the upper *permanent* thermocline as a consequence of subduction, rather than in the *seasonal* thermocline. In response to wintertime atmospheric conditions, large interannual-to-decadal changes in the STMW properties have been reported by Hanawa (1987), Bingham *et al.* (1992), Suga and Hanawa (1995), and Hanawa and Kamada (2001). Notice that enhanced subduction also takes place in regions *downstream* of the Kuroshio Extension where Central and Eastern Mode Waters are formed (Fig. 17(a); Suga *et al.*, 1997; Hautala and Roemmich, 1998). In contrast to these downstream regions where subducted temperature anomalies would move away from their formation region (e.g., Deser *et al.*, 1996, Schneider *et al.*, 1999), Fig. 17(c) shows that the STMW anomalies tend to remain in the recirculation gyres of the Kuroshio and Kuroshio Extension.

From the viewpoint of ocean-atmosphere coupling, it is crucial where the subducted temperature anomalies in the thermocline would be re-exposed through the surface mixed layer to interact with the overlying atmosphere. Gu and Philander (1997) suggested that the temperature anomalies subducted in the midlatitude Central North Pacific could reemerge in the eastern equatorial Pacific Ocean, influence the tropical and midlatitude atmospheric circulations, and give rise to PDOs. Away from the tropics, areas where thermocline water is able to be re-entrained into the wintertime mixed layer (termed “obduction” in Qiu and Huang, 1995) are located in the Kuroshio Extension and Subarctic Frontal Zone regions (see Fig. 17(b)). Physically, obduction occurs preferen-

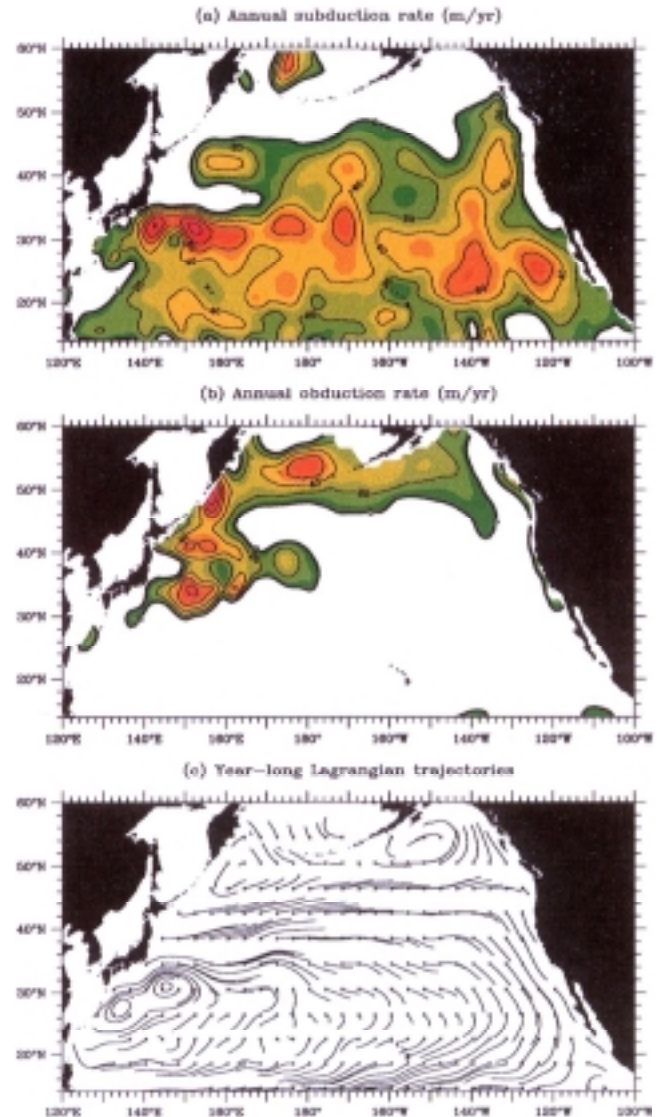


Fig. 17. Annual mean (a) subduction rate and (b) obduction rate. Rates are inferred from the Levitus (1982) temperature/salinity climatology and the Hellerman and Rosenstein (1983) wind stress climatology. (c) Year-long trajectories of water particles released from the base of the late winter (March) mixed layer. The along-isopycnal geostrophic velocities are calculated using the 2000-dbar depth as the reference level. Adapted from Qiu and Huang (1995).

tially in these two regions because of the local misalignment between the steep  $h_m$  gradients and the horizontal velocity vectors of the WBC outflows (see Eq. (2) below). Given the proximity between the subduction and obduction sites in the Kuroshio Extension region, it is likely that changes in the Kuroshio Extension system or in the atmospheric conditions can alter the STMW prop-

erties through subduction, and that the sequestered STMW anomalies can reemerge to influence the SST signals in subsequent winters through obduction.

In the surface ocean heat budget equation (1), the obduction process is associated with the vertical entrainment term\*,  $w_e(T_m - T_d)/h_m$ . By definition, the entrainment velocity (i.e., the mass transfer rate through the base of the mixed layer) is  $w_e \equiv \partial h_m / \partial t + \nabla \cdot (h_m \mathbf{u}_m)$ . Assuming  $\mathbf{u}_m = \mathbf{u}_e + \mathbf{u}_g$  and that the geostrophic velocity  $\mathbf{u}_g$  is effectively nondivergent, we can rewrite  $w_e$  as the sum of three different dynamic processes:

$$w_e = \frac{\partial h_m}{\partial t} + w_{Ek} + \mathbf{u}_g \cdot \nabla h_m. \quad (2)$$

Here,  $\partial h_m / \partial t$  denotes the mixed layer depth change due to the local atmospheric forcing (such as wind stirring and convective cooling),  $w_{Ek} = \nabla \cdot (\boldsymbol{\tau} \times \mathbf{k} / \rho_{df})$  denotes the Ekman pumping velocity, and  $\mathbf{u}_g \cdot \nabla h_m$  denotes the lateral induction rate. Given the in-situ temperature measurements that are available to us at present (e.g., the White (1995) data set is on a  $2^\circ$  lat.  $\times$   $5^\circ$  long. grid), it is very difficult to accurately diagnose the entrainment velocity. Note that the difficulty with  $w_e$  is further exacerbated by the fact that the water temperature just below the base of the mixed layer,  $T_d$ , is also poorly defined from available observational data. In most surface ocean heat budget studies,  $T_d$  was chosen on an *ad hoc* basis (e.g., by setting the temperature difference  $T_m - T_d$  to a predetermined value). At present, while we do know that the mode waters serve as the “memory” of the atmospheric forcing history, we unfortunately do not know the extent to which this oceanic “memory” could re-surface and affect the SST anomalies on the interannual-to-decadal time scales.

## 6. Summary

Being the western boundary current outflow for the North Pacific subtropical circulation, the Kuroshio Extension not only has high mesoscale eddy variability, it also undergoes large-scale transport and path variations on the interannual and longer time scales. Due to its transport of warm waters from the tropics to higher latitudes, the Kuroshio Extension is also where the intense, midlatitude ocean-atmosphere interaction occurs. In this study, we have described the large-scale changes in the

Kuroshio Extension and its recirculation gyre and discussed how the large-scale changes in this system can affect the regional, wintertime surface ocean heat balance. The major points from the study are listed below:

1. The large-scale Kuroshio Extension system oscillates between an elongated and a contracted state. In the elongated state, the Kuroshio Extension has a larger eastward surface transport, a more northerly zonal-mean path, and is accompanied by an intense southern recirculation gyre. In the contracted state, the Kuroshio Extension has a smaller eastward surface transport, a more southerly mean path, and is accompanied by a weaker southern recirculation gyre.

2. The observed changes between the elongated state (1992–1993; 1998–2000) and the contracted state (1994–1995) are found to correlate favorably with the changes in the interior Sverdrup transport at a lag of about six years. However, the amplitude of the Sverdrup transport change underestimates that of the observed Kuroshio Extension transport change by a factor of 38%. This inflated eastward transport of the Kuroshio Extension, following an enhanced interior Sverdrup transport, is consistent with the notion that the enhanced Sverdrup transport increases the low potential vorticity accumulation in the WBC outflow region, intensifying the recirculating flows of the Kuroshio Extension.

3. The surface Kuroshio Extension is *not* simply a well-mixed layer passively responding to heat flux anomalies forced by the atmosphere. On the contrary, the large-scale changes in the Kuroshio Extension system significantly impact the surface ocean heat balance governing the wintertime SST anomalies. Specifically, the nonseasonal geostrophic heat advection works to generate negative (positive) SST anomalies when the Kuroshio Extension system changes from an elongated (contracted) state to a contracted (elongated) state.

4. In addition to horizontal heat advection, changes of the Kuroshio Extension can also influence the surface ocean heat balance by re-exposing mode water temperature anomalies that were subducted over the previous winters. Since the mixed layer depth  $h_m$  is determined by dynamic and thermodynamic processes independent of those determining the flow patterns ( $\mathbf{u}_g$ ) of the Kuroshio Extension, changes in either  $h_m$  or  $\mathbf{u}_g$  can modify the surface ocean heat balance through lateral heat induction.

Much of the discussion presented in this study has been based on the 8-year T/P measurements. Given the long time scale in which the large-scale Kuroshio Extension variability is involved, the conclusions listed above should be viewed as preliminary. Clearly, future studies are needed to extend the time series that describes the large-scale changes in the Kuroshio Extension system. At the same time, enhanced monitoring and process-oriented in-situ studies are required to further our under-

---

\*Vertical entrainment includes emergence to the surface mixed layer of subsurface water from both the *seasonal* and *permanent* thermoclines. Qiu and Huang (1995) defined “obduction” as the emergence of the permanent thermocline water. Unlike the emergence of seasonal thermocline water (see Alexander and Deser, 1995), obduction is largely determined by advection of the geostrophic flow intersecting the base of the mixed layer.

standing of and ability to predict the long-term SST changes in the Kuroshio Extension region. It is encouraging to note that such process-oriented in-situ studies are being proposed and/or planned by both Japanese and U.S. scientists. In addition, the T/P follow-on satellite, Jason-1, is scheduled to be launched in December of 2001. As the Jason-1 altimeter will sample the same ground track as the T/P altimeters, inter-calibratable high-quality SSH data will become available to us in the coming decade. Our understanding of the Kuroshio Extension system, its dynamics and its role in the midlatitude ocean-atmosphere interaction, will undoubtedly improve as the longer, future observational data become available.

### Acknowledgements

I would like to thank Dr. Ichiro Yasuda for inviting me to contribute this article for the 60th anniversary of the Oceanographic Society of Japan. Comments made by Drs. Clara Deser, Kimio Hanawa, and Toshio Suga helped clarify several parts of an earlier version of the manuscript. As a member of a US group advocating the joint US-Japan "Kuroshio Extension System Study (KESS)", I have benefited from many gatherings and in-depth discussions with Drs. Olaf Boebel, Kathy Donohue, Brian Dushaw, Peter Hacker, Bruce Howe, Nelson Hogg, Kathie Kelly, Humio Mitsudera, Randy Watts, and Mark Wimbush. This study was supported by National Science Foundation (OCE-9911268) and by NASA's Jason-1 project (Contract 1207881).

### References

- Adamec, D. (1998): Modulation of the seasonal signal of the Kuroshio Extension during 1994 from satellite data. *J. Geophys. Res.*, **103**, 10,209–10,222.
- Akitomo, K., M. Ooi, T. Awaji and K. Kutsuwada (1996): Interannual variability of the Kuroshio transport in response to the wind stress field over the North Pacific: Its relation to the path variation south of Japan. *J. Geophys. Res.*, **101**, 14,057–14,071.
- Alexander, M. A. and C. Deser (1995): A mechanism for the recurrence of wintertime midlatitude SST anomalies. *J. Climate*, **25**, 122–137.
- Aoki, S., S. Imawaki and K. Ichikawa (1995): Baroclinic disturbances propagating westward in the Kuroshio Extension region as seen by a satellite altimeter and radiometers. *J. Geophys. Res.*, **100**, 839–855.
- Berloff, P. S. and J. C. McWilliams (1999): Large-scale, low-frequency variability in wind-driven ocean gyres. *J. Phys. Oceanogr.*, **29**, 1925–1949.
- Bernstein, R. L. and W. B. White (1981): Stationary and traveling mesoscale perturbations in the Kuroshio Extension current. *J. Phys. Oceanogr.*, **11**, 672–704.
- Bingham, F. M., T. Suga and K. Hanawa (1992): Comparison of upper thermal conditions in the western North Pacific between two pentads: 1938–42 and 1978–82. *J. Oceanogr.*, **48**, 405–425.
- Cayan, D. R. (1992): Latent and sensible heat flux anomalies over the Northern Oceans: Driving the sea surface temperature. *J. Phys. Oceanogr.*, **22**, 859–881.
- Cessi, P., R. V. Condie and W. Young (1990): Dissipative dynamics of western boundary currents. *J. Mar. Res.*, **48**, 677–700.
- Da Silva, A. M., C. C. Young and S. Levitus (1994): *Atlas of Surface Marine Data 1994, Vol. 1: Algorithms and Procedures*. NOAA Atlas NESDIS 6, U.S. Dept. of Commer., Washington, D.C., 83 pp.
- Davis, R. E. (1976): Predictability of sea surface temperature and sea level pressure anomalies over the North Pacific Ocean. *J. Phys. Oceanogr.*, **6**, 249–266.
- Deser, C. and M. L. Blackmon (1995): On the relationship between tropical and North Pacific sea surface variations. *J. Climate*, **8**, 1677–1680.
- Deser, C., M. A. Alexander and M. S. Timlin (1996): Upper-ocean thermal variations in the North Pacific during 1970–1991. *J. Climate*, **8**, 1840–1855.
- Deser, C., M. A. Alexander and M. S. Timlin (1999): Evidence for a wind-driven intensification of the Kuroshio Current Extension from the 1970s to the 1980s. *J. Climate*, **12**, 1697–1706.
- Ebuchi, N. and K. Hanawa (2000): Mesoscale eddies observed by TOLEX-ADCP and TOPEX/POSEIDON altimeter in the Kuroshio recirculation region south of Japan. *J. Oceanogr.*, **56**, 43–57.
- Frankignoul, C. (1985): Sea surface temperature anomalies, planetary waves, and air-sea feedback in the middle latitudes. *Rev. Geophys.*, **23**, 357–390.
- Gu, D. and S. G. H. Philander (1997): Interdecadal climate fluctuations that depend on exchanges between the tropics and extratropics. *Science*, **275**, 805–807.
- Hall, M. M. (1989): Velocity and transport structure of the Kuroshio Extension at 35°N, 152°E. *J. Geophys. Res.*, **94**, 14,445–14,459.
- Hall, M. M. (1991): Energetics of the Kuroshio Extension at 35°N, 152°E. *J. Phys. Oceanogr.*, **21**, 958–975.
- Hanawa, K. (1987): Interannual variations of the winter-time outcrop area of subtropical mode water in the western North Pacific Ocean. *Atmos-Ocean*, **25**, 358–374.
- Hanawa, K. and J. Kamada (2001): Variability of core layer temperature (CLT) of the North Pacific Subtropical Mode Water. *Geophys. Res. Lett.*, **28** (in press).
- Hanawa, K. and L. D. Talley (2001): Mode waters. p. 373–386. In *Ocean Circulation and Climate, Chap. 5.4*, ed. by G. Siedler, J. Church and J. Gould, Academic Press.
- Hautala, S. L. and D. H. Roemmich (1998): Subtropical mode water in the Northeast Pacific Basin. *J. Geophys. Res.*, **103**, 13,055–13,066.
- Hautala, S. L., D. H. Roemmich and W. J. Schmitz, Jr. (1994): Is the North Pacific in Sverdrup balance along 24°N? *J. Geophys. Res.*, **99**, 16,041–16,052.
- Hellerman, S. and M. Rosenstein (1983): Normal monthly wind stress over the world ocean with error estimates. *J. Phys. Oceanogr.*, **13**, 1093–1104.
- Huang, R. X. and B. Qiu (1994): Three-dimensional structure of the wind-driven circulation in the subtropical North Pacific. *J. Phys. Oceanogr.*, **24**, 1608–1622.

- Hurlburt, H. E., A. J. Wallcraft, W. J. Schmitz, P. J. Hogan and E. J. Metzger (1996): Dynamics of the Kuroshio/Oyashio current system using eddy-resolving models of the North Pacific Ocean. *J. Geophys. Res.*, **101**, 941–976.
- Ichikawa, K. and S. Imawaki (1994): Life history of a cyclonic ring detached from the Kuroshio Extension as seen by the Geosat altimeter. *J. Geophys. Res.*, **99**, 15,953–15,966.
- Imawaki, S., H. Uchida, H. Ichikawa, M. Fukasawa, S. Umatani and the ASUKA Group (2001): Satellite altimeter monitoring the Kuroshio transport south of Japan. *Geophys. Res. Lett.*, **28**, 17–20.
- Iwasaka, N. and J. M. Wallace (1995): Large scale air sea interaction in the Northern Hemisphere from a view point of variations of surface heat flux by SVD analysis. *J. Meteor. Soc. Japan*, **73**, 781–794.
- Jacobs, G. A., H. E. Hurlburt, J. C. Kindle, E. J. Metzger, J. L. Mitchell, W. J. Teague and A. J. Wallcraft (1994): Decade-scale trans-Pacific propagation and warming effects of an El Niño warming anomaly. *Nature*, **370**, 360–363.
- Jiang, S., F. F. Jin and M. Ghil (1995): Multiple equilibria, periodic, and aperiodic solutions in a wind-driven, double-gyre, shallow-water model. *J. Phys. Oceanogr.*, **25**, 764–786.
- Joyce, T. M. (1987): Hydrographic sections across the Kuroshio extension at 165°E and 175°W. *Deep-Sea Res.*, **34**, 1331–1352.
- Joyce, T. M. and W. J. Schmitz, Jr. (1988): Zonal velocity structure and transport in the Kuroshio Extension. *J. Phys. Oceanogr.*, **18**, 1484–1494.
- Joyce, T. M., I. Yasuda, Y. Hiroe, K. Komatsu, K. Kawasaki and F. Bahr (2001): Mixing in the meandering Kuroshio Extension and the formation of NPIW. *J. Geophys. Res.* (in press).
- Kalnay, E. and co-authors (1996): The NCEP/NCAR 40-year reanalysis project. *Bull. Amer. Meteor. Soc.*, **77**, 437–471.
- Kawai, H. (1972): Hydrography of the Kuroshio Extension. p. 235–354. In *Kuroshio—Its Physical Aspects*, ed. by H. Stommel and K. Yoshida, University of Tokyo Press.
- Kawai, H. and S. Saitoh (1986): Secondary fronts, warm tongues and warm streamers of the Kuroshio Extension system. *Deep-Sea Res.*, **33**, 1487–1507.
- Kawamura, H., K. Mizuno and Y. Toba (1986): Formation process of a warm-core ring in the Kuroshio-Oyashio frontal zone—December 1982–October 1982. *Deep-Sea Res.*, **33**, 1617–1640.
- Latif, M. and T. P. Barnett (1994): Causes of decadal climate variability over the North Pacific and North America. *Science*, **266**, 634–637.
- Latif, M. and T. P. Barnett (1996): Decadal climate variability over the North Pacific and North America: Dynamics and predictability. *J. Climate*, **9**, 2407–2423.
- Levitus, S. (1982): *Climatological Atlas of the World Ocean*. NOAA Prof. Paper No. 13, U.S. Government Printing Office, Washington, D.C., 173 pp.
- Mantua, N. J., S. R. Hare, Y. Zhang, J. M. Wallace and R. C. Francis (1997): A Pacific interdecadal climate oscillation with impacts on salmon production. *Bull. Amer. Meteor. Soc.*, **78**, 1069–1079.
- McCalpin, J. D. and D. B. Haidvogel (1996): Phenomenology of the low-frequency variability in a reduced-gravity, quasigeostrophic double-gyre model. *J. Phys. Oceanogr.*, **26**, 739–752.
- Miller, A. J., D. R. Cayan, T. P. Barnett, N. E. Graham and J. M. Oberhuber (1994): Interdecadal variability of the Pacific Ocean: model response to observed heat flux and wind stress anomalies. *Climate Dyn.*, **9**, 287–302.
- Miller, A. J., D. R. Cayan and W. B. White (1998): A westward-intensified decadal change in the North Pacific thermocline and gyre-scale circulation. *J. Climate*, **11**, 3112–3127.
- Mitchell, J. L., W. J. Teague, G. A. Jacobs and H. E. Hurlburt (1996): Kuroshio Extension dynamics from satellite altimetry and a model simulation. *J. Geophys. Res.*, **101**, 1045–1058.
- Mizuno, K. and W. B. White (1983): Annual and interannual variability in the Kuroshio Current system. *J. Phys. Oceanogr.*, **13**, 1847–1867.
- Nakamura, H. and A. S. Kazmin (2001): Decadal changes in the North Pacific oceanic frontal zones as revealed in ship and satellite observations. *J. Geophys. Res.* (submitted).
- Nakamura, H., G. Lin and T. Yamagata (1997): Decadal climate variability in the North Pacific during the recent decades. *Bull. Amer. Meteor. Soc.*, **78**, 2215–2225.
- Pedlosky, J. (1987): *Geophysical Fluid Dynamics*. Springer-Verlag, 710 pp.
- Qiu, B. (1995): Variability and energetics of the Kuroshio Extension and its recirculation gyre from the first two-year TOPEX data. *J. Phys. Oceanogr.*, **25**, 1827–1842.
- Qiu, B. (2000): Interannual variability of the Kuroshio Extension system and its impact on the wintertime SST field. *J. Phys. Oceanogr.*, **30**, 1486–1502.
- Qiu, B. and R. X. Huang (1995): Ventilation of the North Atlantic and North Pacific: Subduction vs. obduction. *J. Phys. Oceanogr.*, **25**, 2374–2390.
- Qiu, B. and T. M. Joyce (1992): Interannual variability in the mid- and low-latitude western North Pacific. *J. Phys. Oceanogr.*, **22**, 1062–1079.
- Qiu, B. and K. A. Kelly (1993): Upper ocean heat balance in the Kuroshio Extension region. *J. Phys. Oceanogr.*, **23**, 2027–2041.
- Qiu, B. and W. Miao (2000): Kuroshio path variations south of Japan: Bimodality as a self-sustained internal oscillation. *J. Phys. Oceanogr.*, **30**, 2471–2486.
- Qiu, B., K. A. Kelly and T. M. Joyce (1991): Mean flow and variability in the Kuroshio Extension from Geosat altimetry data. *J. Geophys. Res.*, **96**, 18,491–18,507.
- Qu, T., H. Mitsudera and B. Qiu (2001): A climatology of the Kuroshio/Oyashio system east of Japan. *J. Phys. Oceanogr.*, **31**, 2575–2589.
- Roden, G. I. (1998): Upper ocean thermohaline, oxygen, nutrient, and flow structure near the date line in summer of 1993. *J. Geophys. Res.*, **103**, 12,919–12,939.
- Schmitz, W. J., Jr. (1984): Observations of the vertical structure of the eddy field in the Kuroshio Extension. *J. Geophys. Res.*, **89**, 6355–6364.
- Schmitz, W. J., Jr., P. P. Niiler, R. L. Bernstein and W. R. Holland (1982): Recent long-term moored instrument observations in the western North Pacific. *J. Geophys. Res.*,

- 87, 9425–9440.
- Schmitz, W. J., Jr., P. P. Niiler and C. J. Koblinsky (1987): Two-year moored instrument results along 152°E. *J. Geophys. Res.*, **92**, 10,826–10,834.
- Schneider, N. and A. J. Miller (2001): Predicting western North Pacific Ocean climate. *J. Climate*, **14**, 3997–4002.
- Schneider, N., A. J. Miller, M. A. Alexander and C. Deser (1999): Subduction of decadal North Pacific temperature anomalies: Observations and dynamics. *J. Phys. Oceanogr.*, **29**, 1056–1070.
- Spall, M. A. (1996): Dynamics of the Gulf Stream/deep western boundary current crossover. Part II: Low-frequency internal oscillations. *J. Phys. Oceanogr.*, **26**, 2169–2182.
- Suga, T. and K. Hanawa (1995): Interannual variations of North Pacific subtropical mode water in the 137°E section. *J. Phys. Oceanogr.*, **25**, 1012–1017.
- Suga, T., Y. Takei and K. Hanawa (1997): Thermostat distribution in the North Pacific subtropical gyre: The central mode water and the subtropical mode water. *J. Phys. Oceanogr.*, **27**, 140–152.
- Sugimoto, T., Y. Kawasaki and J. Li (1992): A description of the time-dependent hydrographic structure of the warm streamer around the Kuroshio warm-core ring 86B. *Deep-Sea Res.*, **39**, S77–S96.
- Tai, C.-T. and W. B. White (1990): Eddy variability in the Kuroshio Extension as revealed by Geosat altimetry: Energy propagation away from the jet, Reynolds stress, and seasonal cycle. *J. Phys. Oceanogr.*, **20**, 1761–1777.
- Talley, L. (1997): North Pacific Intermediate Water transports in the mixed water region. *J. Phys. Oceanogr.*, **27**, 1795–1803.
- Talley, L., Y. Nagata, M. Fujimura, T. Iwao, T. Kono, D. Inagake, M. Hirai and K. Okuda (1995): North Pacific Intermediate Water in the Kuroshio/Oyashio mixed water region. *J. Phys. Oceanogr.*, **25**, 475–501.
- Tanimoto, Y., N. Iwasaka, K. Hanawa and Y. Toba (1993): Characteristic variations of sea surface temperature with multiple time scales in the North Pacific. *J. Climate*, **6**, 1153–1160.
- Tatebe, H. and I. Yasuda (2001): Seasonal axis migration of the upstream Kuroshio Extension associated with standing oscillations. *J. Geophys. Res.*, **106**, 16,685–16,692.
- Teague, W. J., M. J. Carron and P. J. Hogan (1990): A comparison between the Generalized Digital Environmental Model and Levitus climatologies. *J. Geophys. Res.*, **95**, 7167–7183.
- Toba, Y., J. Kimura, H. Murakami, M. Kim, Y. Yoshikawa and K. Shimada (2001): Unusual behavior of the Kuroshio current system from winter 1996 to summer 1997 revealed by ADEOS-OCTS and other data (continued): A study from broad external conditions with bottom topography. *J. Oceanogr.*, **57**, 141–154.
- Wang, L., C. J. Koblinsky and S. Howden (1998): Annual and intra-annual sea level variability in the region of the Kuroshio Extension from TOPEX/POSEIDON and Geosat altimetry. *J. Phys. Oceanogr.*, **28**, 692–711.
- White, W. B. (1995): Design of a global observing system for gyre-scale upper ocean temperature variability. *Progr. Oceanogr.*, **36**, 169–217.
- White, W. B. and Y. He (1986): Interannual variability in the heat content of the Kuroshio Extension associated with the 1982 ENSO event. *J. Phys. Oceanogr.*, **16**, 309–321.
- Wijffels, S. E., M. M. Hall, T. Joyce, D. J. Torres, P. Hacker and E. Firing (1998): Multiple deep gyres of the western North Pacific: A WOCE section along 149°E. *J. Geophys. Res.*, **103**, 12,985–13,009.
- Wunsch, C. (1999): Where do ocean eddy heat fluxes matter? *J. Geophys. Res.*, **104**, 13,235–13,249.
- Wyrki, K. (1975): Fluctuations of the dynamic topography in the Pacific Ocean. *J. Phys. Oceanogr.*, **5**, 450–459.
- Wyrki, K., L. Magaard and J. Hagar (1976): Eddy energy in the oceans. *J. Geophys. Res.*, **81**, 2641–2646.
- Xie, P. and P. A. Arkin (1997): Global precipitation: 17-year monthly analysis based on gauge observations, satellite estimates and numerical model outputs. *Bull. Amer. Meteor. Soc.*, **78**, 2539–2558.
- Xie, S.-P., T. Kunitani, A. Kubokawa, M. Nonaka and S. Hosoda (2000): Interdecadal thermocline variability in the North Pacific for 1958–1997: A GCM simulation. *J. Phys. Oceanogr.*, **30**, 2798–2813.
- Yamagata, T., Y. Shibao and S.-I. Umatani (1985): Interannual variability of the Kuroshio Extension and its relation to the Southern Oscillation/El Niño. *J. Oceanogr. Soc. Japan*, **41**, 274–281.
- Yasuda, I. (1997): The origin of the North Pacific Intermediate Water. *J. Geophys. Res.*, **102**, 893–909.
- Yasuda, I., K. Okuda and M. Hirai (1992): Evolution of a Kuroshio warm-core ring—Variability of the hydrographic structure. *Deep-Sea Res.*, **39**, 131–161.
- Yasuda, I., K. Okuda and Y. Shimizu (1996): Distribution and modification of North Pacific Intermediate Water in the Kuroshio-Oyashio inter-frontal zone. *J. Phys. Oceanogr.*, **26**, 448–465.
- Yasuda, I., T. Tozuka, M. Noto and S. Kouketsu (2000): Heat balance and regime shifts of the mixed layer in the Kuroshio Extension. *Progr. Oceanogr.*, **47**, 257–278.
- Yasuda, T. and K. Hanawa (1997): Decadal changes in the mode waters in the midlatitude North Pacific. *J. Phys. Oceanogr.*, **27**, 858–870.
- Zhang, Y., J. M. Wallace and D. S. Battisti (1997): ENSO-life interdecadal variability: 1900–93. *J. Climate*, **10**, 1004–1020.